Pattern Recognition 98 (2020) 107054

Contents lists available at ScienceDirect

Pattern Recognition

journal homepage: www.elsevier.com/locate/patcog

A Möbius transformation based model for fingerprint minutiae variations

James Moorfield[a], Song Wang[b,*], Wencheng Yang[c], Aseel Bedari[b], Peter Van Der Kamp[b]

[a] Viewbank College, Warren Road, Rosanna, VIC 3084, Australia
[b] School of Engineering and Mathematical Sciences, La Trobe University, VIC 3086, Australia
[c] Security Research Institute, Edith Cowan University, WA 6027 Australia

ARTICLE INFO

Article history:
Received 6 March 2019
Revised 27 August 2019
Accepted 12 September 2019
Available online 13 September 2019

Keywords:
Minutiae variations
Fingerprint pattern
Möbius transformation
Minutiae translation
Minutiae rotation
Non-linear distortion

ABSTRACT

When an individual's fingerprint is scanned, although the global fingerprint pattern is unchanged, at the local level, between different scans the minutiae pattern may vary. Minutiae translation and rotation are caused by changing finger orientation and position shift during fingerprint acquisition. Minutiae patterns may also suffer non-linear distortion due to finger skin elasticity. Despite a variety of approaches to detecting deformations in fingerprint images, there has been no method available for capturing minutiae variations between two impressions of the same finger in a unified model. In this paper we address this issue by proposing a unified model to represent minutiae variations between fingerprint scans and formulate the changes to minutiae feature patterns. We identify the Möbius transformation as a good candidate for modelling minutiae translation, rotation and non-linear distortion, that is, different types of minutiae variations are described in a single model. Not only do we mathematically prove that the Möbius transformation based model is a unified model for capturing minutiae variations, but we also experimentally verify the effectiveness of this model using a public database.

1. Introduction

With good recognition accuracy and strong security, fingerprint-based biometric recognition [1] is becoming an appealing alternative to traditional password- and token-based authentication. During fingerprint acquisition, a fingerprint sensor or scanner acquires fingerprint images through some means of contact sensing. The quality of the acquired images can be affected by a number of physiological, behavioral and environment factors, e.g., the amount of pressure applied by the person, the elasticity of finger skin, the disposition of the person (sitting or standing), the moisture content of finger skin (dry, wet or oily), the motion of the finger and ambient temperature and light. As a result, fingerprint images contain a fair amount of uncertainty and variability, giving rise to intra-class variations and inter-class similarity [1]. How to extract more useful information from noisy (or even poor-quality) fingerprint images has attracted intense research interest in the areas of image processing and pattern recognition for many years.

In a fingerprint image, apart from the global fingerprint pattern, such as the ridge line flow, at the local level, minutiae points provide salient information about an individual's fingerprint features [1] and play an important role in the design of fingerprint recognition systems. In particular, in recent years researchers have successfully applied minutia-based local structures [2] to the popular research topic of fingerprint template protection; see e.g., [3–7]. These minutia-based local structures have some desirable properties – they are stable and alignment-free. However, in the fingerprint acquisition process, when a person presses his/her fingertip against the plain surface of a fingerprint scanner, the resultant fingerprint image is produced through a three-dimension(3D)-to-two-dimension(2D) mapping. In this process, minutiae variations occur between different scans, because minutiae points are affected by linear transformations like translation and rotation. Moreover, due to skin elasticity – compression or stretch, minutiae are subject to elastic deformation [8] or non-linear plastic distortion. The ideal way to cope with minutiae variations is to invert the 3D-to-2D mapping and compare minutiae in 3D, but how to invert this mapping has not been found.

A number of techniques have been presented in literature to deal with the issue of minutiae variations (translation, rotation and non-linear distortion) that are inherent in fingerprint images, resulting in different approaches from different perspectives. Bazen

* Corresponding author.
E-mail addresses: james.moorfield@outlook.com (J. Moorfield), song.wang@latrobe.edu.au (S. Wang), w.yang@ecu.edu.au (W. Yang), 18012630@students.latrobe.edu.au (A. Bedari), p.vanderkamp@latrobe.edu.au (P.V.D. Kamp).

https://doi.org/10.1016/j.patcog.2019.107054
0031-3203/

and Gerez [8,9] used a thin-plate spline model to represent non-linear distortion as a non-rigid transformation, which compensates for elastic deformation to improve minutiae matching performance. But this model has to be fitted in rounds of iterations and the accuracy of this model is dependent on the size of the tolerance zone around a minutia. Bolle et al. [10] and Fujii [11] invented hardware-based methods to measure force and torque during fingerprint image capture. These hardware devices are expected to allow contact sensing of fingerprints to be completed with minimal distortion. Specifically, the mechanism designed by Bolle et al. [10] detects and measures excessive force and torque at image acquisition, while the fingerprint distortion detection unit devised by Fujii [11] detects the amount of movement of a finger on a fingerprint sensor through a transparent elastic film or a transparent board, which is mounted on or semi-fixed to the reading face of the fingerprint sensor. These hardware units restrict the application of force to be within a certain range during capturing. The hardware rejects distorted records and prompts the user to provide a new impression until the system requirements are satisfied. There are several drawbacks related to the use of hardware-based distortion detection methods: (a) specific sensors and/or additional instrumentation are required; (b) they cannot handle distorted fingerprint images from previously recorded samples; and (c) the system becomes weak against malicious users who fake their fingertips and ridge patterns.

To study the dynamic behavior of fingerprints, Dorai et al. [12] proposed the use of fingerprint video streams and applied joint temporal and motion analysis to structural distortion detection. Although the proposed approach can reliably detect non-linear plastic distortion of fingerprint impressions and estimate fingerprint positions based on compressed fingerprint videos, the use of streamed video sequences is inefficient or infeasible in the mobile computing environment, where time and energy consumption is highly restrictive. In addition, researchers have come up with various models for non-linear distortion in fingerprint images. Unlike the thin-plate spline model [8,9], Cappelli et al. [13] investigated distortion patterns in different parts of fingerprint images taken with online acquisition sensors. It was revealed in [13] that finger pressure against the sensor surface was non-uniform, decreasing from the finger center towards the outer area. Accordingly, a non-linear distortion model proposed in [13] was based on finger pressure variations in three distinct regions of a fingerprint: close-contact region (i.e., center region), outer region and the region in between. Although this model explains the deformation of fingerprint images caused by improper finger positioning, estimation of model parameters is hard and unreliable. Chen et al. [14] developed a fuzzy theory based algorithm to tackle non-linear distortion. The proposed algorithm can detect spurious minutiae and achieves good recognition accuracy for deformed fingerprints. However, image alignment is a prerequisite for the proposed algorithm, which means that if pre-alignment is wrong, the proposed algorithm cannot perform well.

Despite aforementioned software- and hardware-based approaches to detecting deformations in fingerprint images, there has been no method available for capturing minutiae variations in a unified model. None of the existing models can deal with rigid transformations (e.g., minutiae translation and rotation) and non-rigid transformations (e.g., non-linear distortion) in a comprehensive manner, so that they can be described in a single model. In this paper we address this issue by proposing a unified model, which is able to represent minutiae variations between fingerprint scans and formulate the changes to minutiae feature patterns. By observing the similarity between the process of pressing one's fingertip bulging outwards on a fingerprint scanner and taking objects on a curved surface and mapping them to a plane, we derive a simple model, namely inversion, for non-linear distortion using the Riemann sphere [15]. In addition, we use complex functions to express minutiae translation, rotation and inversion. Furthermore, we identify the Möbius transformation [16] as a candidate for modelling minutiae translation, rotation and non-linear distortion, that is, different types of minutiae variations are described in one, unified model. Not only do we mathematically prove that the Möbius transformation based model is a unified model for capturing minutiae variations, but we also experimentally verify the effectiveness of this model using the public database FVC2002 DB2 [17].

The paper is organized as follows. Section 2 presents the complex functions to describe minutiae translation, rotation and inversion as well as develops the inversion model for non-linear distortion. Section 3 proposes the Möbius transformation based model and proves why it can be used to model minutiae variations. In Section 4, we evaluate the efficacy of the Möbius transformation based model through experiments conducted over the public database FVC2002 DB2 [17]. The conclusion and future work are given in Section 5.

2. Minutiae translation, rotation and non-linear distortion

Minutiae variations that occur to different fingerprint scans include translation, rotation and non-linear distortion. Translations and rotations are due to changing finger orientation and position shift at fingerprint capturing time, while non-linear distortion is introduced by variable skin pressure. In this section, we propose inversion as a simple model for non-linear distortion.

Minutiae translation, rotation and inversion can be described by complex-valued functions. In order to use these functions, a minutia's position is represented by a complex number z, which means that the co-ordinates (x, y) of the minutia are given by $x = \mathrm{Re}(z)$ and $y = \mathrm{Im}(z)$, where $\mathrm{Re}(z)$ is the real part of z and $\mathrm{Im}(z)$ is the imaginary part of z. We now introduce the complex functions that express these mappings.

Proposition 1. *A translation in the complex plane is represented by a function of the form*

$$f(z) = z + \gamma \tag{1}$$

where $\gamma \in \mathbb{C}$.

Proof. Observe that $\mathrm{Re}(\gamma)$ displaces z along the real axis and $\mathrm{Im}(\gamma)$ displaces along the imaginary axis, the desired result follows. □

Proposition 2. *Rotation is described by*

$$f(z) = \alpha z \tag{2}$$

where $\alpha \in \mathbb{C}$.

Proof. It is straightforward to prove the result when we express z and α in polar form. □

Non-linear distortion is inevitable during fingerprint capture. However, we notice that pressing our fingerprint on a scanner is similar to mapping points of a curved surface, e.g., a sphere, to a plane. Motivated by this observation, we propose a model for non-linear distortion based on projecting points in the $x - y$ plane to the surface of the Riemann sphere [15]. Consider the surface of the Riemann sphere Σ of unit radius, centred at the origin in $\mathbb{R}^3$. Let Π be the $x - y$ plane and N denote the point (0,0,1). The complex number $z = x + iy$ can be represented by the point $P = (x, y)$ in Π. P can be mapped uniquely to the point P^* by taking the intersection of the line segment NP with Σ, or its extension for P

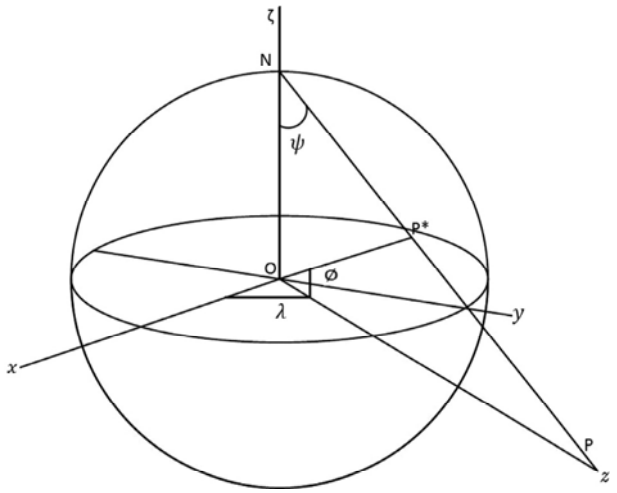

Fig. 1. Projection of point P (i.e., $z = x + iy$) to the Riemann sphere.

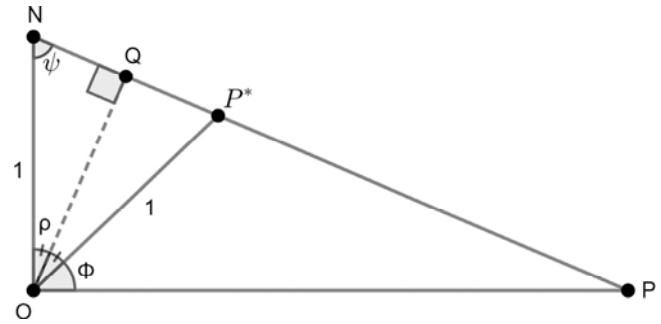

Fig. 2. Triangle NOP.

inside Σ. The point P^* can be represented by overlaying a spherical co-ordinate system, where $\lambda \in (-\pi, \pi]$ and $\phi \in (-\pi/2, \pi/2)$. This arrangement is shown in Fig. 1.

Fig. 2 shows the triangle NOP, where O is the origin. Let $\psi = \angle ONP$ and Q be the point that bisects the line segment NP^*. As NOP^* is an isosceles triangle by construction, the line segment QO bisects $\angle P^*ON$. Let $\rho = \angle NOQ = (\angle P^*ON)/2$. As NOP is a right-angled triangle, we have $\rho = \pi/4 - \phi/2$. We now derive ψ in terms of ϕ as follows:

$$\begin{aligned}\psi &= \frac{\pi}{2} - \rho \\ &= \frac{\pi}{4} + \frac{\phi}{2}\end{aligned}$$

We can now express the point P, represented by $z = x + iy$, with respect to our spherical co-ordinates λ and ϕ. Observe $\arg z = \lambda$ and $|z| = \tan\psi$. Therefore,

$$z = \tan\left(\frac{\pi}{4} + \frac{\phi}{2}\right)e^{i\lambda} \tag{3}$$

Proposition 3. *Let g denote the function that rotates the sphere Σ by angle π about the x-axis. Let h map the points in the $x-y$ plane Π to the sphere Σ, as discussed above. Inversion is described by $f(z) = h^{-1} \circ g \circ h(z)$, where the symbol $\circ$ denotes function composition, and*

$$f(z) = 1/z \tag{4}$$

Proof. Observe rotation about the real axis corresponds to rotation about the x-axis in Fig. 1. After rotation of the sphere, $\phi \to -\phi$ and $\lambda \to -\lambda$. Using (3), we have

$$\begin{aligned}f(z) &= \tan\left(\frac{\pi}{4} - \frac{\phi}{2}\right)e^{-i\lambda} \\ &= \frac{\sin\left(\frac{\pi}{4} - \frac{\phi}{2}\right)}{\cos\left(\frac{\pi}{4} - \frac{\phi}{2}\right)}e^{-i\lambda} \\ &= \frac{\sin\frac{\pi}{4}\cos\frac{\phi}{2} - \cos\frac{\pi}{4}\sin\frac{\phi}{2}}{\cos\frac{\pi}{4}\cos\frac{\phi}{2} + \sin\frac{\pi}{4}\sin\frac{\phi}{2}}e^{-i\lambda} \\ &= \frac{\cos\frac{\pi}{4}\cos\frac{\phi}{2} - \sin\frac{\pi}{4}\sin\frac{\phi}{2}}{\sin\frac{\pi}{4}\cos\frac{\phi}{2} + \cos\frac{\pi}{4}\sin\frac{\phi}{2}}e^{-i\lambda} \\ &= \frac{\cos(\frac{\pi}{4} + \frac{\phi}{2})}{\sin(\frac{\pi}{4} + \frac{\phi}{2})}e^{-i\lambda} \\ &= \frac{1}{\tan(\frac{\pi}{4} + \frac{\phi}{2})\,e^{i\lambda}} \\ &= \frac{1}{z}\end{aligned}$$

□

We have shown that inversion corresponds to projection from a rotation of the Riemann sphere. Figs. 3 and 4 illustrate the effect of inversion on a collection of example points in $\mathbb{C}$ that lie in a square.

Remark. In practice, since fingerprint acquisition is normally a monitored process, the amount of non-linear distortion should be less drastic than that shown in Figs. 3 and 4.

3. The Möbius transformation based model

Based on the above analysis, we now introduce the Möbius transformation and show that it renders a good candidate for modelling minutiae variations between two impressions of the same finger.

Definition. A mapping of the form

$$f(z) = \frac{az + b}{cz + d} \tag{5}$$

is called a *Möbius transformation* [18], where $a, b, c, d \in \mathbb{C}$, and $ad - bc \neq 0$.

Note that the assumption $ad - bc \neq 0$ is necessary [16] because if $ad - bc = 0$, the mapping $f(z)$ in (5) becomes a constant mapping, sending every point z to the same image point a/c.

Despite its seemingly simplicity, the Möbius transformation has abundant applications in fields such as computer vision and biological image analysis, thanks to its beautiful properties and ability to work with non-Euclidean geometry. For example, in order to identify possible transformations in different images of the same object, Marsland and Mclachlan [19] presented Möbius invariants for both curves and images as well as developed invariant signatures, by which shapes can be recognised. In the context of building a model for fingerprint minutiae variations, we shall prove that the Möbius transformation (5) can represent minutiae translation, rotation and non-linear distortion.

Theorem. *The Möbius transformation is composed of translation, rotation and inversion.*

Proof. Let $f(z)$ be a Möbius transformation as defined in (5).

Case 1: $c = 0$. This implies $f(z) = (a/d)z + b/d$. Let $f_1 = (a/d)z$ and $f_2 = z + b/d$. Thus,

$$f_2 \circ f_1 = (a/d)z + b/d = f(z)$$

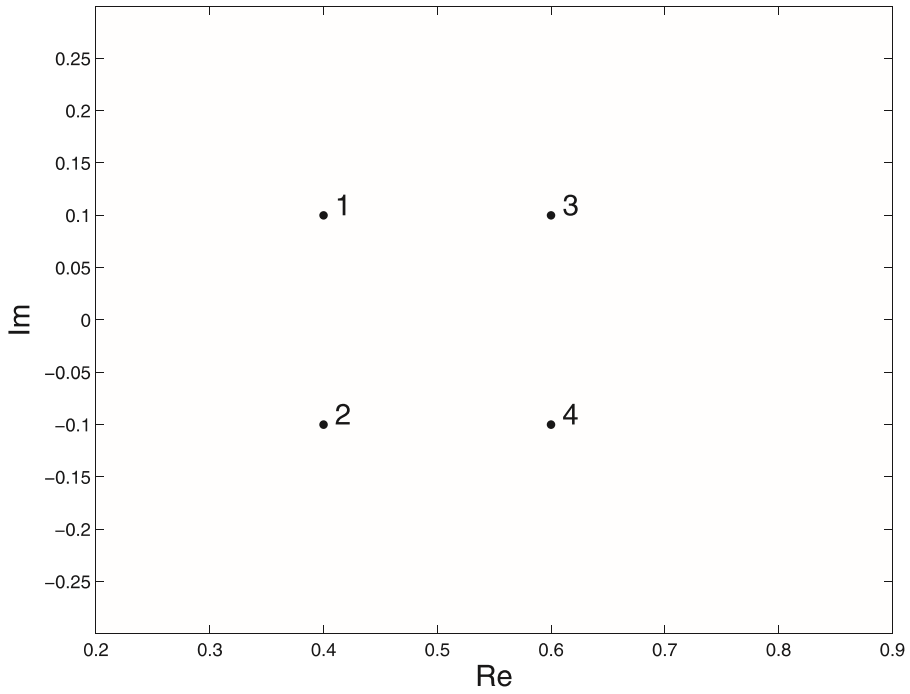

Fig. 3. Before inversion.

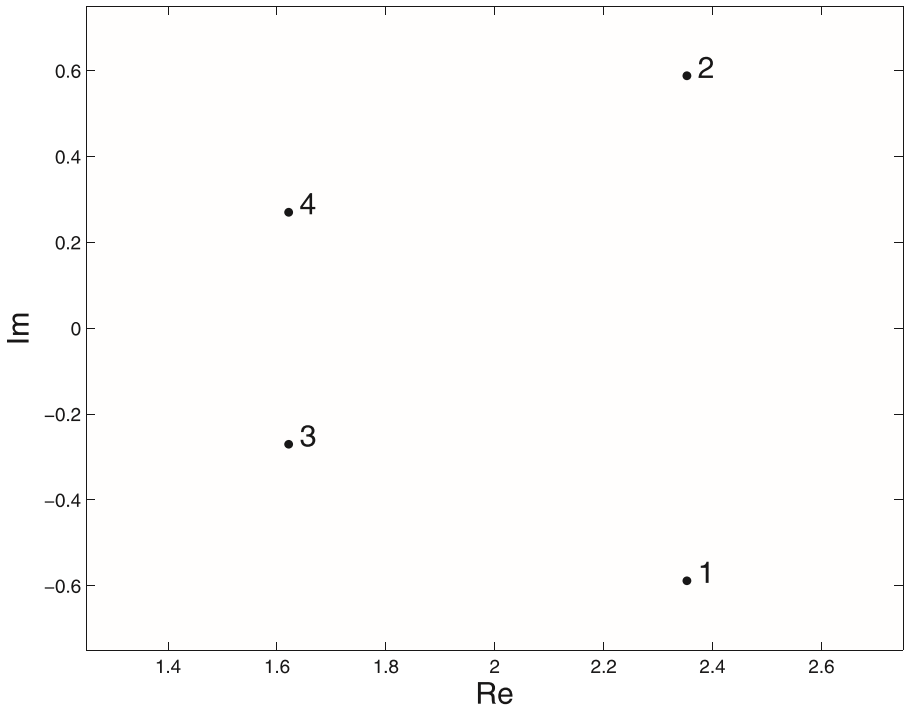

Fig. 4. After inversion.

In this case, it follows from Propositions 1 and 2 that f is composed of translation and rotation.

Case 2: $c \neq 0$. According to [18], suppose $f_1(z) = z + d/c$, $f_2(z) = 1/z$, $f_3(z) = \frac{(bc-ad)}{c^2} z$ and $f_4(z) = z + a/c$. Based on Propositions 1, 2 and 3, these functions describe translation, rotation and inversion.

$$f_2 \circ f_1 = 1/(z + d/c)$$

$$\Rightarrow f_3 \circ f_2 \circ f_1 = \frac{bc - ad}{(cz + d)c}$$

$$\Rightarrow f_4 \circ f_3 \circ f_2 \circ f_1 = \frac{bc - ad}{c(cz + d)} + \frac{a(cz + d)}{c(cz + d)} = \frac{c(az + b)}{c(cz + d)} = f(z)$$

Therefore, $f(z)$ is composed of translation, rotation and inversion as required. □

Our proof above also echos the statement made by Needham [16] that the Möbius transformation can be decomposed into the following fundamental transformations:

i. $z \longmapsto z + \frac{d}{c}$, which is a translation.
ii. $z \longmapsto \frac{1}{z}$, which is inversion.
iii. $z \longmapsto -\frac{ad-bc}{c^2} z$, which is a rotation.
iv. $z \longmapsto z + \frac{a}{c}$, which is another translation.

In addition, it is shown [16] that there exists a unique Möbius transformation mapping any three given points to three other given points. Three points form a triangle and we know that triangles play a special role in Euclidean geometry, which is underpinned by similarity transformations. However, for similarities to exist in the realm of Euclidean geometry, the image points must form a triangle that is similar to the triangle formed by the original points, so this is considered as a type of rigid transformation. On the other hand, such similarities can be expressed by complex functions of the form $f(z) = az + b$, which is exactly a simplified version of the Möbius transformation (5). It is noted that minutiae translation and rotation can be dealt with by rigid transformations using Euclidean geometry, whereas non-linear distortion is caused by finger skin elasticity and such elastic deformation has to be treated by more flexible, non-Euclidean geometries through non-rigid transformations. The Möbius transformation fulfills that role. In other words, the Möbius transformation suits both rigid and non-rigid transformations.

The Möbius transformation possesses some nice properties [16] that are beneficial for modelling minutiae variations. These properties are:

- The Möbius transformation is conformal because it preserves local angles.
- The Möbius transformation preserves symmetry. Here, symmetry means that if two points are symmetric with respect to a circle, then their images under the Möbius transformation are symmetric with respect to the image circle.
- The Möbius transformation is bijective (i.e., one-to-one and onto). This property can be shown by finding the inverse function of (5):

$$f^{-1}(z) = \frac{dz - b}{-cz + a}$$

It follows that $f^{-1}(z)$ is also a Möbius transformation.

We have proved mathematically that the Möbius transformation is a suitable candidate for modelling minutiae translation and rotation as well as non-linear distortion described by inversion. In the next section, we carry out experiments using the public database FVC2002 DB2 [17] to test the effectiveness of the proposed Möbius transformation based model.

4. Experimental results and discussion

To evaluate how effective the Möbius transformation based model is when modelling minutiae variations, we performed testing over the public database FVC2002 DB2 [17]. It is a standard database widely used in fingerprint-based biometrics research. This database contains a sample size of 100 fingers with eight impressions per finger. The minutiae points from the fingerprint images were extracted using the commercial fingerprint recognition software VeriFinger SDK [20]. We assume that the first impression of each finger is the template T and the second impression of the same finger is the query Q.

In order to test whether the proposed model can capture minutiae variations accurately enough, we take the following steps in our experiments:

1. Find the matching minutiae between two impressions of the same finger so that we obtain the reference positions of matching minutiae for subsequent comparisons.
2. From the matching minutiae found in Step 1, work out the amount of minutiae variations between the template fingerprint T and the query fingerprint Q. Specifically, determine the coefficients a, b, c, d of the Möbius transformation (5) by using three randomly selected minutiae in T and their matching minutiae in Q.
3. Based on the values of a, b, c, d, use the minutiae in T to calculate their position-varied minutiae counterpart in Q, or equivalently, the matching minutiae in Q modelled by the Möbius transformation.
4. Compare the modelled minutiae's positions against the minutiae's actual (reference) positions in Q to assess the performance of our Möbius transformation based model.

For Step 1, to determine the matching minutiae between two impressions of the same finger, we applied the pair-minutiae vector based matching method in [4]; refer to Section 3.3 of [4] for the details on matching score calculation. For convenience, we use Finger 7 and Finger 40 to demonstrate our test results. The first impression of Finger 7 and Finger 10, respectively, is considered as the template T and the second impression of the same finger as the query Q.

Although it seems that in order to determine the coefficients a, b, c, d of the Möbius transformation (5), we would need four distinct minutiae (i.e., four different complex numbers) in the template T and the four matching minutiae in the query Q, it turns out that multiplying the coefficients by an arbitrary constant k, where $k \neq 0$, yields the same mapping:

$$\frac{az + b}{cz + d} = f(z) = \frac{kaz + kb}{kcz + kd}$$

Therefore, the coefficients a, b, c, d of the Möbius transformation are non-unique – only the ratios of the coefficients matter [16] and three matching minutia pairs are sufficient to pin down the ratios. That is why in Step 2, we randomly selected only three minutiae rather than four in the template T and their three matching minutiae in the query Q to seek the coefficients a, b, c, d.

First, we report the experimental results of Finger 7. Fig. 5 shows some examples of matching minutiae from Finger 7. By employing the matching mechanism in [4], we found the matching minutia pairs. Some of the matched pairs are listed in Table 1; for example, pairs $1-2$, $3-11$, $6-5$ and $9-6$ in the template T

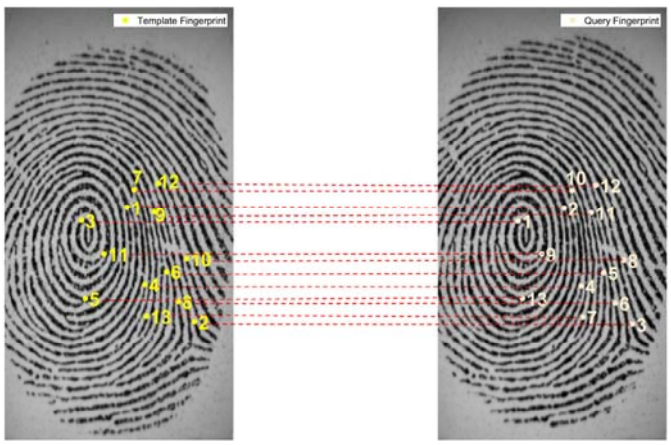

Fig. 5. Examples of matching minutiae between the template T and the query Q of Finger 7. (Note: For the sake of clarity, this figure only shows a portion of the minutiae in Finger 7.)

Table 1
Matched minutia pairs of Finger 7 and comparison of the modelled minutiae (last column) with the actual query minutiae (second last column).

Template T		Matched Query Q		Modelled
Minutia pair	Minutia position	Minutia pair	Minutia position	minutia pair
1	$159+260i$	2	$\mathbf{164+261i}$	$\mathbf{164.2+261.0i}$
2	$246+408i$	3	$\mathbf{252+411i}$	$\mathbf{252.4+411.2i}$
2	$246+408i$	3	$\mathbf{252+411i}$	$\mathbf{252.4+411.2i}$
6	$210+343i$	5	$\mathbf{215+344i}$	$\mathbf{215.3+344.1i}$
9	$194+266i$	11	$\mathbf{199+267i}$	$\mathbf{198.8+266.8i}$
8	$225+382i$	6	$\mathbf{230+384i}$	$\mathbf{230.6+384.1i}$
3	$100+277i$	1	$\mathbf{104+278i}$	$\mathbf{106.1+277.2i}$
11	$129+320i$	9	$\mathbf{135+320i}$	$\mathbf{134.1+320.1i}$
12	$199+229i$	12	$\mathbf{205+231i}$	$\mathbf{203.3+230.2i}$
4	$182+360i$	4	$\mathbf{186+362i}$	$\mathbf{186.6+361.3i}$
9	$194+266i$	11	$\mathbf{199+267i}$	$\mathbf{198.8+266.8i}$
6	$210+343i$	5	$\mathbf{215+344i}$	$\mathbf{215.3+344.1i}$
7	$168+237i$	10	$\mathbf{174+238i}$	$\mathbf{173.1+238.4i}$
8	$225+382i$	6	$\mathbf{230+384i}$	$\mathbf{230.6+384.1i}$
9	$194+266i$	11	$\mathbf{199+267i}$	$\mathbf{198.8+266.8i}$
10	$236+326i$	8	$\mathbf{241+328i}$	$\mathbf{241.7+326.7i}$
6	$210+343i$	5	$\mathbf{215+344i}$	$\mathbf{215.3+344.1i}$
5	$105+378i$	13	$\mathbf{110+378i}$	$\mathbf{108.4+377.5i}$
1	$159+260i$	2	$\mathbf{164+261i}$	$\mathbf{164.2+261.1i}$
11	$129+320i$	9	$\mathbf{135+320i}$	$\mathbf{134.1+320.1i}$
12	$199+229i$	12	$\mathbf{205+231i}$	$\mathbf{203.3+230.2i}$
13	$184+401i$	7	$\mathbf{188+402i}$	$\mathbf{188.1+403.2i}$

Table 2
Matched minutia pairs of Finger 40 and comparison of the modelled minutiae (last column) with the actual query minutiae (second last column).

Template T		Matched Query Q		Modelled
Minutia pair	Minutia position	Minutia pair	Minutia position	minutia pair
1	$142+271i$	2	$\mathbf{140+284i}$	$\mathbf{138.8+284.4i}$
2	$221+275i$	1	$\mathbf{218+296i}$	$\mathbf{216.7+295.8i}$
3	$131+265i$	4	$\mathbf{128+277i}$	$\mathbf{128.4+277.3i}$
4	$93+320i$	3	$\mathbf{84+328i}$	$\mathbf{84.0+328.6i}$
3	$131+265i$	4	$\mathbf{128+277i}$	$\mathbf{128.4+277.3i}$
5	$229+333i$	6	$\mathbf{219+353i}$	$\mathbf{220.1+354.0i}$
6	$111+240i$	5	$\mathbf{112+251i}$	$\mathbf{111.5+250.1i}$
5	$229+333i$	6	$\mathbf{219+353i}$	$\mathbf{220.1+354.0i}$
7	$117+156i$	8	$\mathbf{126+170i}$	$\mathbf{127.9+168.5i}$
8	$37+310i$	7	$\mathbf{30+313i}$	$\mathbf{28.0+311.6i}$
9	$173+174i$	10	$\mathbf{177+192i}$	$\mathbf{179.8+192.8i}$
4	$93+320i$	3	$\mathbf{84+328i}$	$\mathbf{84.0+328.6i}$
10	$167+196i$	9	$\mathbf{168+213i}$	$\mathbf{171.5+213.5i}$
11	$112+342i$	12	$\mathbf{101+351i}$	$\mathbf{101.1+353.1i}$
9	$173+174i$	10	$\mathbf{177+192i}$	$\mathbf{179.8+192.8i}$
11	$112+342i$	12	$\mathbf{101+351i}$	$\mathbf{101.1+353.1i}$
15	$177+219i$	13	$\mathbf{178+237i}$	$\mathbf{178.8+236.9i}$
3	$131+265i$	4	$\mathbf{128+277i}$	$\mathbf{128.4+277.3i}$
7	$117+156i$	8	$\mathbf{126+170i}$	$\mathbf{127.9+168.5i}$
12	$66+246i$	11	$\mathbf{66+252i}$	$\mathbf{65.8+250.5i}$
13	$176+461i$	14	$\mathbf{156+475i}$	$\mathbf{157.6+481.1i}$
14	$138+481i$	15	$\mathbf{113+490i}$	$\mathbf{116.1+499.9i}$

match with pairs $2-3$, $1-9$, $5-13$ and $11-5$ in the query Q, respectively.

The matching minutiae could be readily obtained from those matched minutia pairs. After identifying the matched pairs, we should be able to work out the minutiae variations between two matching minutiae through the Möbius transformation. Eq. (5) was used to numerically calculate the amount of variations occurred between the matching minutiae in the template T and the query Q. That is, we should determine the coefficients a, b, c and d in (5), where $f(z)$ is set as the minutia position in Q and z as the minutia position in T. If we refer to Table 1, the minutiae's positions of the first two pairs (containing three distinct minutiae 1, 2 and 6) in T and their corresponding matching minutiae (2, 3 and 5) in Q are used to find a, b, c and d, which yield $a = 0.8851 - 0.0019i$, $b = 14.9744 + 18.1392i$, $c = 0.000087467 + 0.00013611i$, $d = 1$. We then substitute these values of a, b, c and d into (5) and use the minutiae in T from Table 1 to calculate the modelled minutiae $f(z)$. The comparison between $f(z)$ and the actual query minutiae's po-

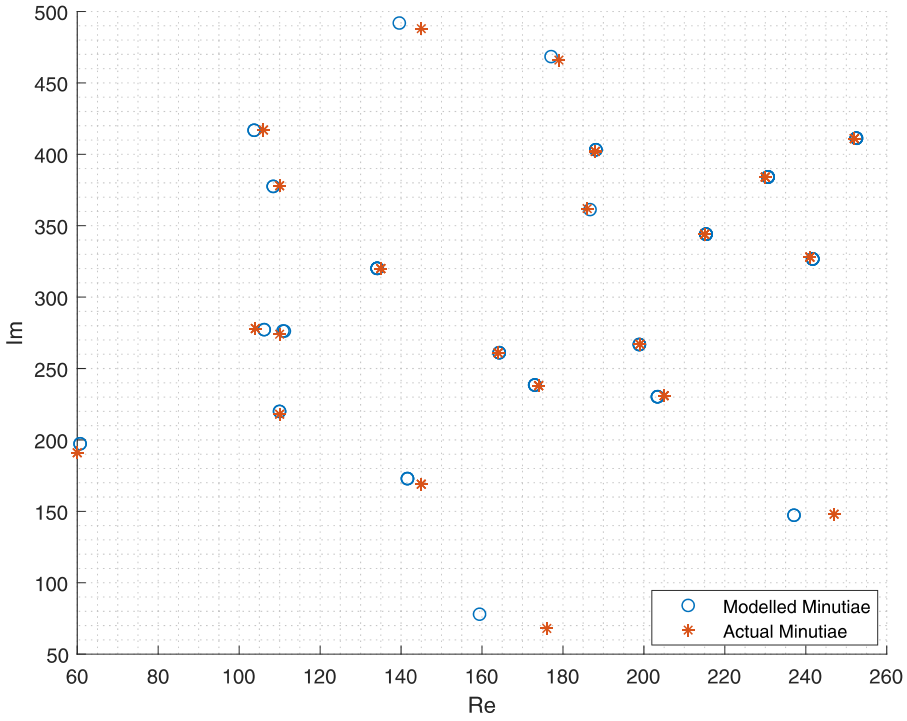

Fig. 6. Comparison of the modelled minutiae with the actual query minutiae of Finger 7.

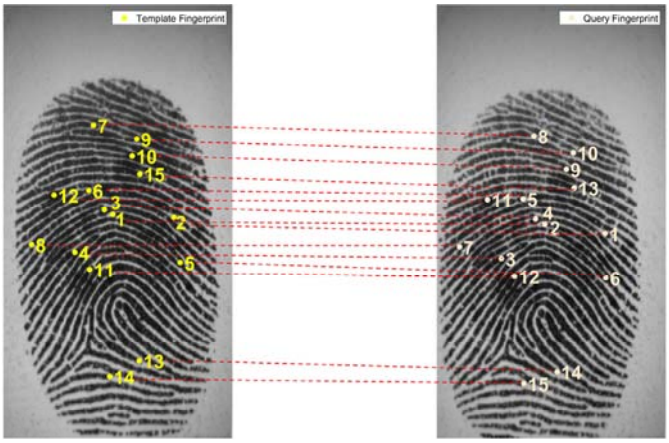

Fig. 7. Examples of matching minutiae between the template T and the query Q of Finger 40. (Note: For the sake of clarity, this figure only shows a portion of the minutiae in Finger 40.)

sitions in Q should reveal the performance of the proposed model. This comparison is shown by the last two columns of Table 1, from which we can see that $f(z)$ obtained from the Möbius transformation based model is quite close to the actual query minutiae.

In Fig. 6, we plot the minutiae's positions modelled by the Möbius transformation, in comparison with the actual minutiae in the query Q of Finger 7. It is clear that a majority of minutiae calculated from the Möbius transformation based model fall in the proximity of actual query minutiae. These results demonstrate that the Möbius transformation can model minutiae variations effectively between two impressions of the same finger.

Next, we report the test results of Finger 40. Fig. 7 shows some matching minutiae between the template T and the query Q of this finger. The matching minutiae were obtained from the matched minutia pairs, which followed the same method in [4] as used for Finger 7. Table 2 lists some of the matching minutia pairs of Finger 40; for example, pairs $15-3$, $3-4$, $13-14$ and $7-8$ in the template T match with pairs $13-4$, $4-3$, $14-15$ and $8-7$ in the query Q, respectively. By randomly selecting the second and third minutia pairs in T (consisting of minutiae 3, 4 and 5) and their matching minutiae 4, 3 and 6, the same procedure for Finger 7 was applied to Finger 40 to find the coefficients a, b, c and d in the Möbius transformation, resulting in $a = 0.9450 + 0.1934i$, $b = 40.8843 + 1.3577i$, $c = 0.00010239 + 0.00012495i$ and $d = 1$. After substituting these values of a, b, c and d into (5), we calculated the modelled minutiae $f(z)$ by setting z in (5) as the minutiae in the template T from Table 2. It can be observed from the last two columns of Table 2 that the modelled minutiae through the Möbius transformation are very similar to the actual query minutiae in terms of minutia position. This similarity is also exhibited clearly in Fig. 8.

The main computations incurred by the proposed method are: (i) calculating the coefficients a, b, c, d of the Möbius transformation (5); and (ii) determining the modelled minutiae based on a, b, c, d and the (known) minutiae in the template. One way to quantify the amount of arithmetic involved is to count flops. A flop [21] is a floating point add, subtract, multiply or divide. The values of a, b, c, d are obtained by calculating the determinants of four 3×3 matrices [16], amounting to 56 flops in total. After a, b, c, d are found, using the template minutiae, we can calculate the modelled minutiae according to (5). To acquire a modelled minutia only requires 5 flops. Obviously, the total amount of arithmetic work in the proposed method is low. All of these results are obtained using Matlab, which is run on a PC with Core i7, 3.41 GHz CPU and Operation System of 64-bit Win 10. It takes 0.0057 s to calculate a, b, c, d for all of 100 fingers in the database FVC2002 DB2 [17]. It costs 0.0539 s to determine the modelled minutiae for 100 fingers of the same database. Thus, the proposed method is computationally inexpensive.

The forensic guidelines require that to decide if it is the same finger, the minimum number of matching minutiae should be 12 according to [22]. From Tables 1 and 2, which only include a portion of the matched minutia pairs, we can see that the number of

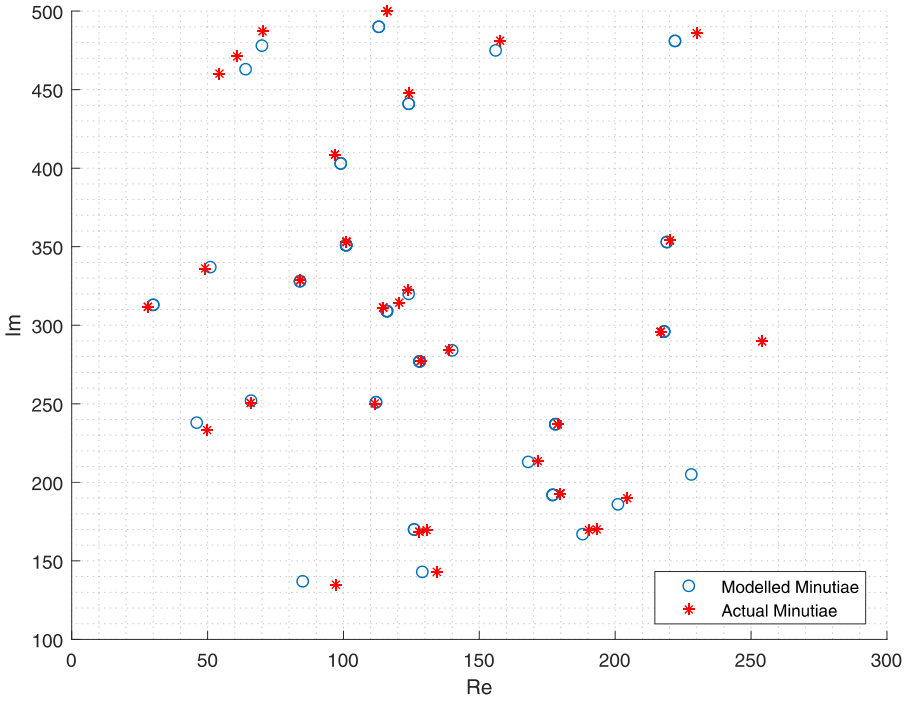

Fig. 8. Comparison of the modelled minutiae with the actual query minutiae of Finger 40.

Table 3
The average Euclidean distance (in pixels) between the actual and modelled minutiae of each finger in the database FVC2002 DB2 (100 fingers).

Finger 1	Finger 2	Finger 3	Finger 4	Finger 5	Finger 6	Finger 7
1.235	1.365	1.429	1.297	1.334	2.256	0.559
Finger 8	Finger 9	Finger 10	Finger 11	Finger 12	Finger 13	Finger 14
1.813	1.903	0.674	1.433	1.707	1.425	2.658
Finger 15	Finger 16	Finger 17	Finger 18	Finger 19	Finger 20	Finger 21
0.891	6.464	1.636	1.616	1.535	2.592	1.050
Finger 22	Finger 23	Finger 24	Finger 25	Finger 26	Finger 27	Finger 28
1.209	0.729	1.023	0.772	1.874	1.957	3.661
Finger 29	Finger 30	Finger 31	Finger 32	Finger 33	Finger 34	Finger 35
1.256	0.440	0.925	1.013	0.646	1.134	1.073
Finger 36	Finger 37	Finger 38	Finger 39	Finger 40	Finger 41	Finger 42
3.053	0.976	1.209	1.065	0.800	0.966	1.150
Finger 43	Finger 44	Finger 45	Finger 46	Finger 47	Finger 48	Finger 49
0.891	0.787	1.159	0.895	0.950	0.678	1.185
Finger 50	Finger 51	Finger 52	Finger 53	Finger 54	Finger 55	Finger 56
0.779	0.641	1.142	0.527	2.938	0.940	0.652
Finger 57	Finger 58	Finger 59	Finger 60	Finger 61	Finger 62	Finger 63
2.415	1.414	0.531	1.861	0.699	0.885	1.118
Finger 64	Finger 65	Finger 66	Finger 67	Finger 68	Finger 69	Finger 70
1.341	0.708	0.417	1.285	1.547	1.325	0.414
Finger 71	Finger 72	Finger 73	Finger 74	Finger 75	Finger 76	Finger 77
0.756	0.354	4.409	0.763	0.578	0.803	0.649
Finger 78	Finger 79	Finger 80	Finger 81	Finger 82	Finger 83	Finger 84
0.831	1.724	0.984	0.512	0.404	1.397	1.336
Finger 85	Finger 86	Finger 87	Finger 88	Finger 89	Finger 90	Finger 91
1.927	0.794	0.918	1.474	2.576	0.463	1.121
Finger 92	Finger 93	Finger 94	Finger 95	Finger 96	Finger 97	Finger 98
1.306	0.990	0.811	2.425	0.918	3.021	1.024
Finger 99	Finger 100					
0.984	1.194					

matching minutiae is much greater than 12 and that our Möbius transformation based model accurately captures minutiae variations between two impressions of the same finger.

To thoroughly evaluate the proposed method, we conducted further testing over the entire database FVC2002 DB2 [17] with a total of 100 fingers. The forensic guidelines [22] require at least 12 mated pairs to make a 'match' verdict on two fingerprints, so we found 12 best matched minutia pairs between the template (i.e, the first impression) and the query (i.e., the second impression of the same finger) for each finger in the database FVC2002 DB2 [17] by applying the matching approach in [4]. We then calculated the Euclidean distance between the actual and modelled minutiae. That is, the Euclidean distance between the (actual) minutia (x_1, y_1) and its modelled minutia (x_2, y_2) is $d = \sqrt{(x_2 - x_1)^2 + (y_2 - y_1)^2}$. The average Euclidean distance between these actual and modelled minutiae is reported in Table 3. From

the Euclidean distance in Table 3, it is clear that the modelled and actual minutiae are very close to each other. Therefore, we have experimentally verified the validity of the proposed model.

5. Conclusion

It is well known that minutiae variations occur to different impressions of the same finger. How to capture these variations between fingerprint scans is a research problem of theoretical and practical importance, yet a unified model for describing minutiae variations has not been available. In this paper we have proposed the Möbius transformation based model as a unified model to express minutiae variations – translation, rotation and non-linear distortion. We prove mathematically that the Möbius transformation based model is a unified model for representing different types of minutiae variations. In addition, we use the public database FVC2002 DB2 [17] to evaluate the effectiveness of the proposed model. The experimental results show that the modelled minutiae through the Möbius transformation are very close to the actual minutiae in terms of minutia position, which verifies the efficacy of the proposed model.

The Möbius transformation based model provides a useful tool for the analysis and construction of minutia-based local feature structures. As for future work, we will continue to improve this model and investigate how to efficiently apply it to enhancing the quality and accuracy of minutia extraction in modern-day fingerprint-based biometric applications, e.g, e-passports, mobile device authentication and mobile healthcare data protection.

References

[1] D. Maltoni, D. Maio, A.K. Jain, S. Prabhakar, Handbook of Fingerprint Recognition, second ed., Springer, 2009.
[2] A.K. Jain, K. Nandakumar, A. Nagar, Fingerprint template protection: from theory to practice, in: Security and Privacy in Biometrics, Springer-Verlag, 2013, pp. 187–214. Chapter 8.
[3] W. Yang, J. Hu, S. Wang, A Delaunay quadrangle-based fingerprint authentication system with template protection using topology code for local registration and security enhancement, IEEE Trans. Inf. Forensics Secur. 9 (7) (2014) 1179–1192.
[4] S. Wang, J. Hu, Design of alignment-free cancelable fingerprint templates via curtailed circular convolution, Pattern Recognit. 47 (3) (2014) 1321–1329.
[5] S. Wang, J. Hu, A blind system identification approach to cancelable fingerprint templates, Pattern Recognit. 54 (2016) 14–22.
[6] Z. Jin, A.B.J. Teoh, B.M. Goi, Y.H. Tay, Biometric cryptosystems: a new biometric key binding and its implementation for fingerprint minutiae-based representation, Pattern Recognit. 56 (8) (2016) 50–62.
[7] S. Wang, W. Yang, J. Hu, Design of alignment-free cancelable fingerprint templates with zoned minutia pairs, Pattern Recognit. 66 (2017) 295–301.
[8] A.M. Bazen, S.H. Gerez, Elastic minutiae matching by means of thin-plate spline models, in: Proceedings of the Sixteenth IEEE International Conference on Pattern Recognition, volume 2, 2002, pp. 985–988.
[9] A.M. Bazen, S.H. Gerez, Fingerprint matching by thin-plate spline modelling of elastic deformations, Pattern Recognit. 36 (8) (2003) 1859–1867.
[10] R.M. Bolle, R.S. Germain, R.L. Garwin, J.L. Levine, S.U. Pankanti, N.K. Ratha, M.A. Schappert, System and method for distortion control in live-scan inkless fingerprint images, 2000. U.S. Patent 6064753, granted May 16.
[11] Y. Fujii, Detection of fingerprint distortion by deformation of elastic film or displacement of transparent board, 2010. U.S. Patent 7660447, granted February 9.
[12] C. Dorai, N.K. Ratha, R.M. Bolle, Dynamic behavior analysis in compressed fingerprint videos, IEEE Trans. Circ. Syst. Video Technol. 14 (1) (2004) 58–73.
[13] R. Cappelli, D. Maio, D. Maltoni, Modelling plastic distortion in fingerprint images, in: Proceedings of the International Conference on Advances in Pattern Recognition, 2001, pp. 369–376. March 11–14.
[14] X. Chen, J. Tian, X. Yang, A new algorithm for distorted fingerprints matching based on normalized fuzzy similarity measure, IEEE Trans. Image Process. 15 (3) (2006) 767–776.
[15] R.A. Silverman, Introductory Complex Analysis, Prentice-Hall, 1967.
[16] T. Needham, Visual Complex Analysis, Oxford University Press, 1997.
[17] Fingerprint verification competition, 2002. http://bias.csr.unibo.it/fvc2002/.
[18] J.B. Conway, Functions of One Complex Variable I, Springer-Verlag, 1978.
[19] S. Marsland, R.I. Mclachlan, Möbius invariants of shapes and images, Symmetry Integr. Geom Methods Appl. SIGMA volume 080 (2016) 29. 12.
[20] Neurotechnology, VeriFingerSDK (http://www.neurotechnology.com/megamatcher.html).
[21] G.H. Golub, C.F.V. Loan, Matrix Computations, fourth ed., Johns Hopkins University Press, 2013.
[22] T.Y. Jea, V. Govindaraju, A minutia-based partial fingerprint recognition system, Pattern Recognition 38 (10) (2005) 1672–1684.

James Moorfield is currently a mathematics teacher at Viewbank College, Melbourne, Australia.

Song Wang received the B.Eng. (Electrical Engineering) from Xi'an Jiaotong University, China and Ph.D. from the University of Melbourne, Australia. She worked as a design engineer at NEC Australia in 2000–2004. Since January 2005 she has been with the Department of Engineering, La Trobe University, Australia, where she is currently a Senior Lecturer. Her research areas include biometric security, pattern recognition and blind channel estimation.

Wencheng Yang is a postdoctoral researcher with the Security Research Institute (SRI) at Edith Cowan University, Australia. His major research interest is in biometric security and pattern recognition. He has several papers published in high-ranking journals such as IEEE Transactions on Information Forensics and Security and Pattern Recognition.

Aseel Bedari is a Ph.D. student in the Department of Engineering, La Trobe University, Australia. Her research interest is biometric security.

Peter van der Kamp's main research interests lie in the field of integrable systems, a broad area at the boundary of physics and mathematics. He is mainly concerned with algebraic and geometric properties of nonlinear differential equations and difference equations.